Monatshefte für Chemie - Chemical Monthly (2023) 154:367–377
https://doi.org/10.1007/s00706-023-03055-6

ORIGINAL PAPER

# Polyethylenimine-grafted graphene oxide: a versatile photothermal nanocomposite for catalysis and carbon dioxide capture-and-release under simulated and natural sunlight

**Xuejing Guo[1] · Yewen Zhang[1] · Yanqing Peng[1]**

Received: 26 September 2022 / Accepted: 10 March 2023 / Published online: 28 March 2023


## Abstract

Application of solar thermal energy relies on photothermal effect is one of the emerging topics in green chemical research. Polyethylenimine-grafted graphene oxide (PEI@GO) can harvest thermal energy directly from visible light and be employed as photothermal catalyst in model reactions. Furthermore, this nanocomposite used in carbon dioxide capture-and-release processes relied on photothermal regeneration.

### Graphical abstract

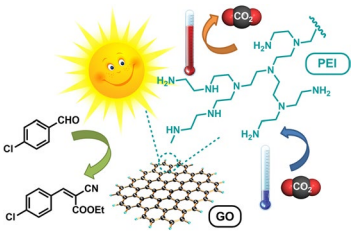


**Keywords** Solar energy · Photothermal nanocomposite · Graphene oxide · Polyethylenimine · Catalysis · Desorption

## Introduction

Radiant energy from the sun hits the earth in wavelengths in orders ranging from 0.1 to 10 mm. Solar energy is a renewable source of sufficient scale to meet rising global energy demand over the century [1]. Therefore, solar energy has become a promising alternative resource better than fossil fuels. On the other hand, the variances in temperature alter the rate of a chemical reaction. Usually, an increase in temperature is accompanied by acceleration in the reaction rate. As a reasonable inference, the use of solar thermal energy is advantageous from the viewpoint of green synthesis and sustainable chemistry.

✉ Yanqing Peng
yqpeng@ecust.edu.cn

[1] Shanghai Key Laboratory of Chemical Biology, School of Pharmacy, East China University of Science and Technology, Shanghai 200237, China

In the past decade, materials for light-to-heat conversion are widely used in biomedical research [2]. Photothermal therapy is a promising antitumor strategy that employs photo-absorbing agents to burn cancer cells by heat generated from optical energy [3]. Recently, photothermal technology has been employed in chemistry and chemical engineering. In a recent review, the applications of plasmonic metals, semiconducting and their hybrid materials in catalysis and evaporation have been described in detail [4–7].

Noble metal nanoparticles, such as gold and silver, present unique optical properties given their strong interaction with visible and near-infrared (NIR) light. This coupling gives an effect known as localized surface plasmon resonance (LSPR) [8]. Plasmon-induced chemistry becomes a hot topic of research relies on the LSPR effect to enhance chemical reactions [9, 10]. Sun and co-works report the integration of plasmonic Au nanorods with catalytic Pd nanoparticles enabled efficient light harvesting for Suzuki

coupling reaction under laser (809 nm). Moreover, similar yield was also obtained using Au–$TiO_x$–Pd nanostructures under the same laser illumination [11]. Pd nanostructures [12] and Pd@$Nb_2O_5$ [13] were revealed efficient photothermal catalysts for hydrogenation.

As a novel family of two-dimensional materials, graphene and graphene oxide (GO) have received much interest. Among their interesting electric, mechanical, thermal, and chemical properties [14], the photothermal conversion is one of the most important properties for graphene and GO. Therefore, they have been applied in photothermal therapy [15] and research fields of chemistry. Designed nanocomposites, plasmonic metal nanoparticles supported on graphene, show synergistic effects in catalysis of various reactions. Under near-infrared irradiation or visible light, the reduction rate of nitro compound was significantly enhanced by the heating of local environment around metal nanoparticles in Cu nanoparticles/reduced graphene oxide nanocomposite [16] and dumbbell-like Au nanorods supported on graphene/$TiO_2$ sheets [17]. Similarly, other types of photothermal catalysts including Au/reduced graphene oxide (oxidation of benzylic alcohols) [18], Pd(II)- and Pd(0)-loaded GO/r-GO (Suzuki–Miyaura coupling) [19], graphene oxide coupled with Ag and $Fe_3O_4$ nanopaticles composites (oxidation of cyclohexane) [20] have been reported in literatures.

It needs to be emphasized that graphene itself has no special effect based on localized surface plasmon resonance. Compared to nanosized metals with LSPR effect, therefore, graphene has attracted much less attention in photothermal catalysis. Graphene-based $MnO_2$ nanohybrid has recently been prepared and investigated under irradiation of a xenon lamp for catalytic oxidation of gaseous formaldehyde. The excellent activity was attributed to the synergistic effect between $MnO_2$ and graphene [21]. To the best of our knowledge, however, there is no description on the use of graphene-immobilized organocatalyst in photothermal catalysis.

In addition, there has been a rapid growth in research activities for carbon dioxide capture and utilization due to it is one of the major greenhouse gases and a major contributor to global climate change. Esser-Kahn and co-workers have recently reported the use of photothermal technology in carbon dioxide capture-and-release processes [22]. Carbon dioxide was captured by aqueous monoethanolamine solution under relatively low temperatures. Carbon black nanoparticles absorb light and convert it to thermal energy, and regenerate $CO_2$ capture liquids under bulk temperature of 50 °C. Compared to capture solution, solid adsorbent is more convenient for $CO_2$ capture [23]. For example, the problems of equipment corrosion and relatively low thermal stability of liquid amines, especially in the presence of oxygen or other gases, such as $SO_2$, $NO_2$, and NO, could be overcome by solid adsorbents. In addition, lower energy consumption for $CO_2$ regeneration is needed using solid adsorbents in comparison with liquid ones [24, 25]. Up to now, photothermal regeneration of $CO_2$ from amine-functioinalized solid adsorbent has not been described. In comparison with traditional regeneration process based on fossil energy [26, 27], reasonably, photothermal regeneration process will be more environmentally friendly and energy efficient.

Herein we wish to report our preliminary investigation on the application of polyethylenimine-grafted graphene oxide (PEI@GO) as a versatile photothermal nanocomposite for catalysis and carbon dioxide capture-and-release under simulated and natural sunlight. Graphene oxide serves as not only the support of polyethylenimine (a high-loading polyimino resin), but also the absorber of solar energy for photothermal heating.

## Results and discussion

### Preparation and characterization of polyethylenimine-grafted graphene oxide (PEI@GO)

In the present study, the PEI-grafted graphene was prepared through a two-step process as described in Scheme 1. First, naturally abundant graphite powder was used as a cheap precursor to prepare graphene oxide. GO was prepared according to the improved Hummer's method [28], and the GO powder was obtained after washing, sonication, and vacuum-drying. Next the as-prepared GO was reacted sequentially with $SOCl_2$ and PEI. Following sonication for exfoliation of graphite oxide, the carboxylic groups on the edges of GO sheet was transformed to acyl chloride groups by treatment with $SOCl_2$ under nitrogen atmosphere. Acylated graphene oxide was then grafted with PEI to obtain the target material.

During the transformation of carboxyl to acyl chloride groups, the dispersion of GO turned from brownish yellow to black (Scheme 1, chromophotographic inset B). GO can be chemically reduced by classical reductants, such as hydrazine. Since the bond energy of a C–S bond is weaker than that of a C–N bond, sulfur-containing compounds might to be employed as a more efficient reducing agent in comparison with hydrazine. Yan's group has demonstrated that some sulfur-containing compounds, such as $SO_2$ and $SOCl_2$, could reduce GO to rGO [29]. This fact could be used to explain the phenomenon of color change.

Both the as-prepared GO and PEI-grafted GO exist as loose powders without obvious aggregates. In general, GO refers to the exfoliated graphite oxide, existing in the form of single or few layer nanosheets. Graphite oxide can be conveniently exfoliated to produce colloidal suspensions of GO by simple sonication. The morphological structures of graphene oxide and PEI@GO were measured by means of transmission electron microscopy. The TEM micrograph

**Scheme 1**

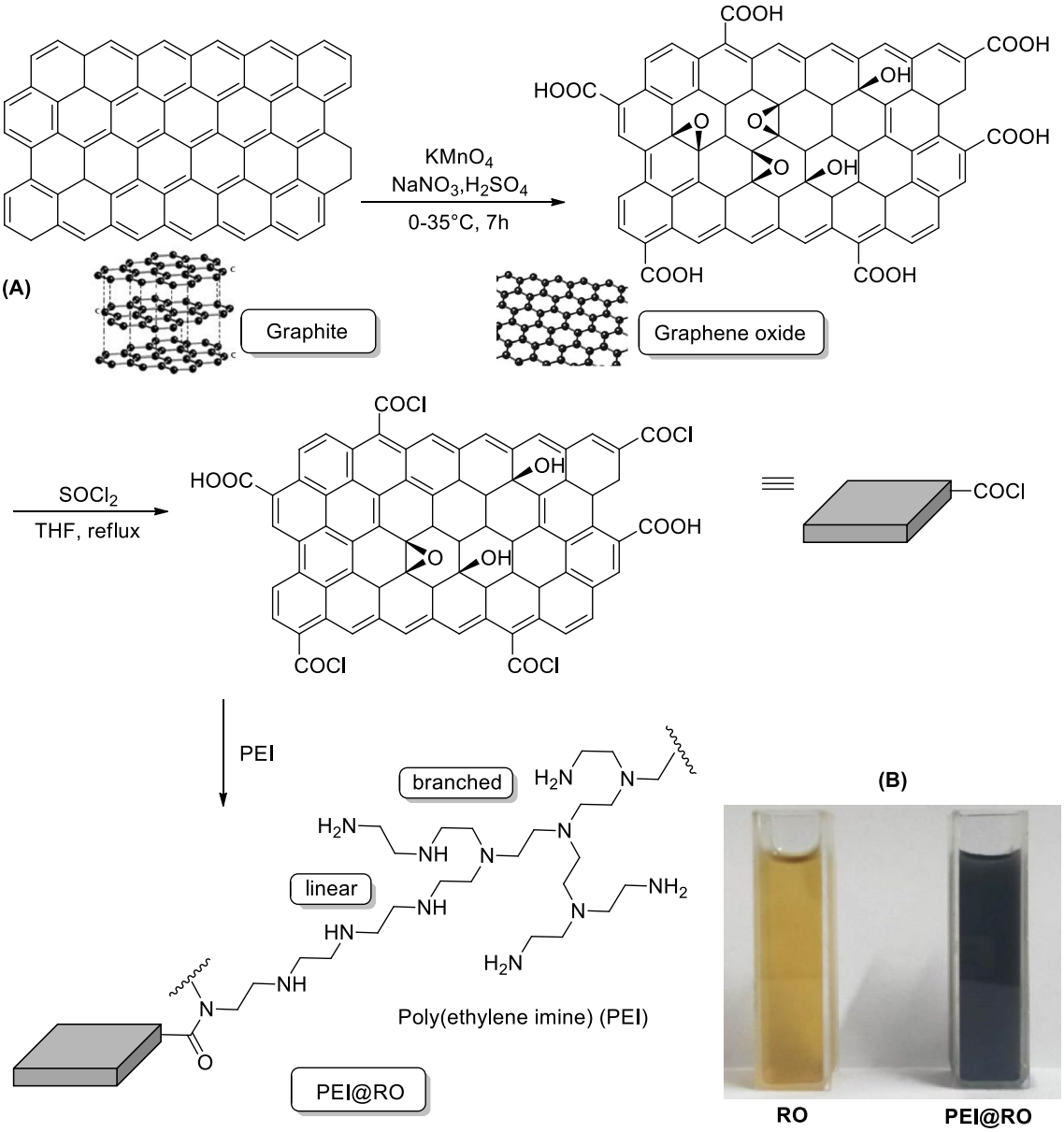


**Fig. 1** TEM images of graphene oxide (**A**) and PEI@GO (**B**) nanosheets

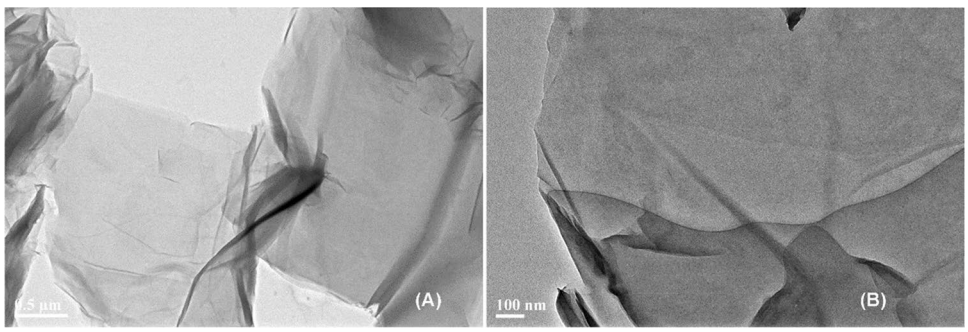

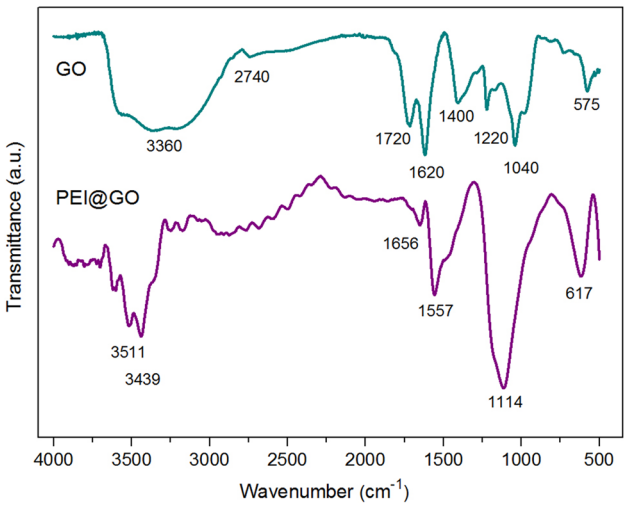


**Fig. 2** FT-IR spectra of GO and PEI@GO

from Fig. 1 clearly showed that the GO and PEI@GO consisted of flakes with wrinkles, and the high transparency observed was attributed to the successful exfoliation.

Fourier transform infrared (FT-IR) spectroscopic characterization of GO and PEI@GO was recorded to reveal the interaction between PEI and GO supporter. As presented in Fig. 2, these two materials exhibit distinctly different FT-IR spectra. The spectrum of GO (cyan curve) shows the broad peak located at 3360 $cm^{-1}$ is associated with the O–H stretching vibration. The band at 1720 $cm^{-1}$ is attributes to the C=O stretching vibration in COOH groups. The peak at 1400 $cm^{-1}$ is bending vibration of hydroxyl groups [3]. In addition, the sharp peak at 1620 $cm^{-1}$ corresponds to the C=C stretching vibration. The absorption band at 1040 $cm^{-1}$ is the attributed to the alkoxy groups (C–O) stretching vibration and the band at 1220 $cm^{-1}$ is the related to the epoxy groups (C–O–C) stretching vibration. These results confirmed that GO contained abundant hydrophilic groups, such as –OH, –COOH, and C–O–C. Those results are in well agreement with the spectra of GO with previous reports [30].

In the spectrum of PEI@GO (purple curve), the absorption peak located at 3439 $cm^{-1}$ corresponds to the N–H stretching vibration. Another important observation is related to the disappearance of the band at 1720 $cm^{-1}$, referring to the C=O vibration of carboxylic acids and the appearance of new bands in the region between 1557 and 1656 $cm^{-1}$, as well as new bands appear at 1656 $cm^{-1}$ (–CONH amide band I) and 1565 $cm^{-1}$ (–NH amide band II). The disappearance of the signal at 1220 $cm^{-1}$ (C–O–C, epoxy) suggests the reactions of epoxides during acyl chloride preparation, namely, ring-opening reaction of epoxides with sulfur-containing reductants followed by aromatization [29]. In the spectra, attached to the alkoxy peak is a signal at 1114 $cm^{-1}$ which is the result of bending vibrations in C–N bonds within PEI polymer [31]. Accordingly, these vibrational characteristics demonstrate that PEI has been successfully grafted onto the GO supporter. The amino group density of PEI@GO was determined to be 5.4 mmol/g by acid–base titration analysis (difference method, indicator phenolphthalein). The amine content was further estimated by elemental analysis. From the result of nitrogen content, we calculated an amine group loading of 5.9 mmol/g. The value of 5.4 mmol/g was used for further dosing accountability.

Figure 3 shows the X-ray diffraction (XRD) patterns of as-synthesized GO and PEI-modified graphene nanosheets. The characteristic diffraction peak at around $2\theta = 10°$ corresponding to the (002) reflects to GO. Meanwhile, the (002) reflection of graphite at $2\theta = 26.5°$ (standard JCPDS file no. 75–2078) is not observed. These facts indicate the complete oxidation of graphite [32]. The diffraction peaks of GO were sharp and intense, indicating their highly crystalline nature. No impurity peaks were observed, confirming the high purity of the products. In XRD pattern of PEI@GO, a broad peak centered at 23.2° was appeared which could be attributed to the conjugation of amorphous polymer. This broadening and shifting could be due to the successfully synthesized PEI@GO nanocomposites.

UV–Vis absorption spectra of GO and PEI@GO recorded in ethanol ($10^{-5}$ mg/$dm^3$). Figure 4 illustrates the absorption of GO includes two typical features, a peak at 230 nm corresponding to the $\pi \rightarrow \pi^*$ transition of the C=C bond, while the observed shoulder peak around 300 nm was attributed to $n \rightarrow \pi^*$ transition of the carbonyl groups. They are in accord with the reported value in the literature [33]. In comparison with GO, PEI@GO has better absorption in whole measurement range, due perhaps to the partial reduction of GO during modification. It is clear that PEI@GO shows potential ability as efficient photothermal material.

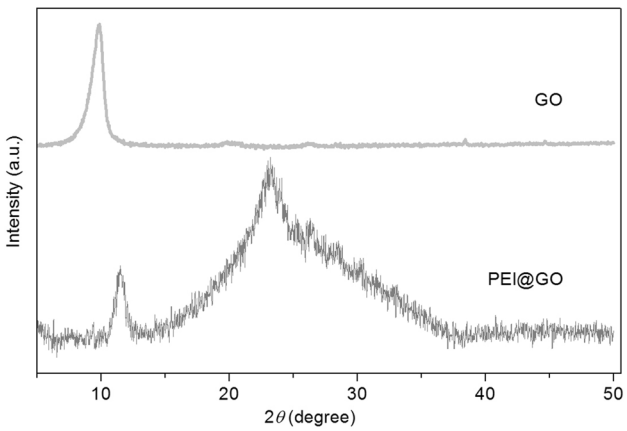


**Fig. 3** XRD patterns of graphene oxide and PEI@GO

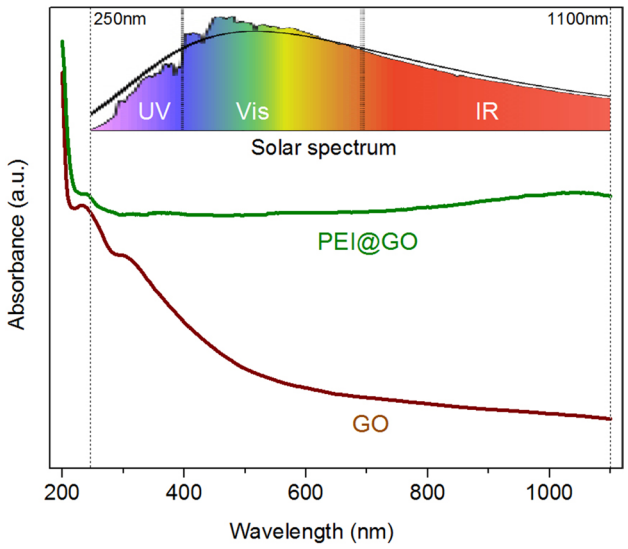


**Fig. 4** UV–Vis absorption spectroscopy of the GO and PEI@GO. Inserted imaging is the solar spectrum from 250 to 1100 nm

Thermogravimetric analysis (TGA) curve showed the mass loss of organic materials as they decompose upon heating. To investigate the thermal behavior of PEI@GO, TGA was carried out under nitrogen atmosphere with a heating rate of 10 °C/min over the temperature range from 40 to 800 °C (Fig. 5). The weight loss below 150 °C is due to the removal of physically adsorbed water. Followed weight loss of 18% in the range of 285–545 °C was contributed to the thermal decomposition of PEI.

As mentioned above, PEI@GO has a wide UV–Vis absorption range, and has high absorption during NIR region which can generate sufficient heat. Photothermal performance of PEI@GO was measured according to standard method [34]. Various amounts of PEI@GO was dispersed

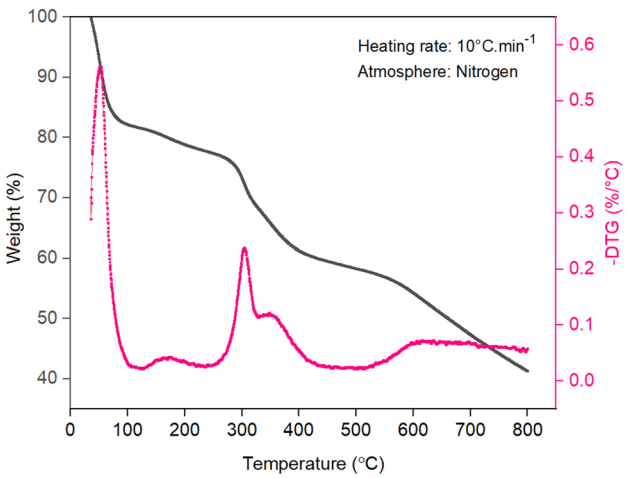


**Fig. 5** TGA and DTG curves of PEI@GO

in ethanol and irradiated by NIR laser (wavelength 808 nm, power 1 W/cm$^2$). The sample was tested under the condition of ambient temperature 20.1 °C, and the result is shown in Fig. 6A. The light-to-heat conversion capacity of the sample progresses with the increase in concentration, and the temperature of samples generally reached a plateau after 6 min. At this moment, the heat generated by the dispersion liquid absorbs light energy and the heat lost to the environment reaches a balance. After 10 min under laser irradiation, the temperature of control sample (pure ethanol without PEI@GO) changed from 19.5 to 21.1 °C. Namely, only negligible temperature elevation ($\Delta T = 1.6$ °C) could be measured. The temperature elevation $\Delta T = 19.1$ °C could be observed in the sample with concentration of 5 mg/cm$^3$. It should be noted that the light-to-heat conversion will not continue to increase with higher sample concentration. Figure 6B shows the repeatability of the photothermal conversion ability of the material (5 mg/cm$^3$). After six cycles, the photothermal conversion ability of the material will not decrease.

## Experiments under simulated and natural sunlight

With PEI@GO in hand, we turned out attention on its potential in photothermal catalytic reactions. Amino-grafted graphene has been reported as a stable and metal-free solid basic catalyst [35]. Initially, Knoevenagel reaction between 4-chlorobenzaldehyde and ethyl cyanoacetate was selected

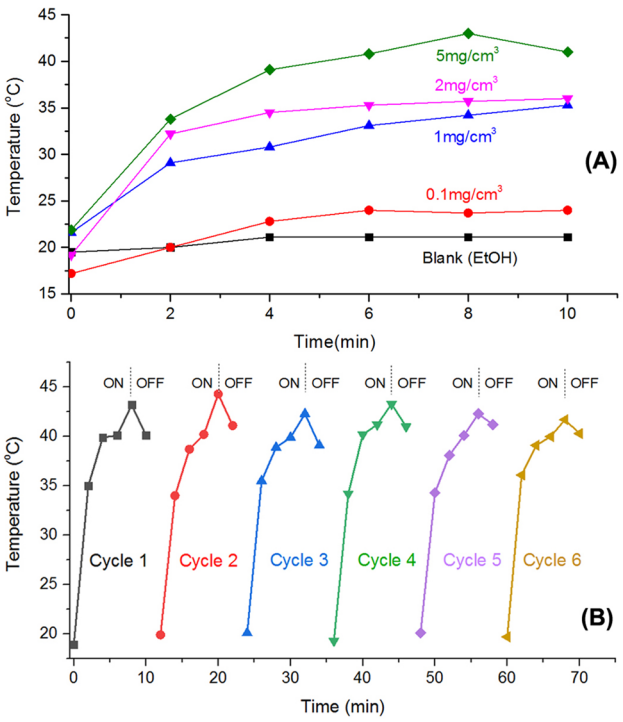


**Fig. 6** Photothermal performance tests (**A**) and heating cycles (**B**) of PEI@GO

as a model reaction. First, condition screening was investigated under conventional oil bath heating. Amount of PEI@GO was investigated in the range of 2–10 mol% relative to 4-chlorobenzaldehyde (Table 1, entries 1–5). In terms of yield and reaction time, 10 mol% of catalyst was considered as the optimum amount.

Second, model reactions were performed under simulated sunlight. Reaction set for experiments could be shown in Fig. 7A. We used 200 W full spectrum LED lamp as light sources to simulate the solar light and use a small parabolic dish concentrator to focus the light in the experiment. By using parabolic dish concentrator, the larger thermodynamic efficiency and the smaller absorbing surface area produced by the increase in operating temperature and amount of heat collected per unit area results in a significant decrease in heat losses [36]. To solve the problem of heat loss, moreover, a foamed polystyrene box was placed outside the reaction system. During reactions, the distance between the full spectrum LED lamp and the bottom of the glass reactor was 20 cm and the solar insolation was measured as 428.6 W/cm$^2$.

The photothermal effect of the catalyst was investigated using solar simulator, and the results are shown in Fig. 8A. Without additional heating, the temperature of the reaction mixture (Table 1, entry 6) can reach up to 69.5 °C and remain on a plateau ($\Delta T_1 = 49$ °C). The control sample (Table 1, entry 9; without catalyst candidate) also showed a temperature rise due to the adsorption of solar energy, but the temperature elevation rise was relatively slow and the plateau temperature was only 44.5 °C ($\Delta T_2 = 24$ °C). Therefore, 10 mol% of PEI@GO shows efficient catalytic activity and good photothermal conversion ability. Polyethylenimine is a classic catalyst for Knoevenagel reaction and, however, has no photothermal conversion ability (Table 1, entry 7). On the contrary, graphene oxide is a satisfactory photothermal agent with poor catalytic activity in model reaction. Infrared thermography transfers invisible infrared radiation into color images and videos taken of reactions and processes. By using infrared camera, real-time images could illuminate the inner temperature of vessels containing PEI@GO, GO, PEI and blank sample, successively (Fig. 8B).

Neonicotinoid insecticides, which act agonistically on the insect nicotinic acetylcholine receptors (nAChRs) [37], play an important role in agricultural production due to their high potency, low mammalian toxicity as well as broad insecticidal spectra. However, a well-recognized potential problem facing all insecticides is the insects' acquisition of resistance. Moreover, the bee toxicity of neonicotinoid insecticides has also attracted extensive attention. Hence, it is necessary to develop new nicotine compounds with novel structure and unique action sites to solve these problems. Our laboratory has reported new neonicotinoid analogues bearing a

**Table 1** Screening of optimal conditions in model reactions

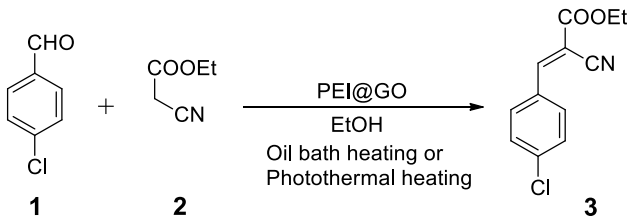


1 2 3

| Entry[a] | Catalyst | Amount of catalyst/mol% | Heating mode | *T*/°C | Time/h | Yield/% |
|---|---|---|---|---|---|---|
| 1 | PEI@GO | 2 | Conventional | Reflux | 8.5 | 88[b] |
| 2 | PEI@GO | 4 | Conventional | Reflux | 8.5 | 86[b] |
| 3 | PEI@GO | 6 | Conventional | Reflux | 8.5 | 91[b] |
| 4 | PEI@GO | 8 | Conventional | Reflux | 3.5 | 92[b] |
| 5 | PEI@GO | 10 | Conventional | Reflux | 3 | 90[b] |
| 6 | PEI@GO | 10 | Photothermal | 69.5 | 6 | 94[b] |
| 7 | PEI | 10 | Photothermal | 42.0 | 6 | 72[c] |
| 8 | GO | 1.4 g[d] | Photothermal | 66.0 | 6 | 28[c] |
| 9 | Blank | 0 | Photothermal | 44.5 | 6 | 22[c] |

[a]Reaction conditions: 4-chlorobenzaldehyde (2 mmol), ethyl cyanoacetate (2.4 mmol), 3 cm$^3$ of EtOH

[b]Isolated yield

[c]GC yield

[d]Weight of catalyst support GO

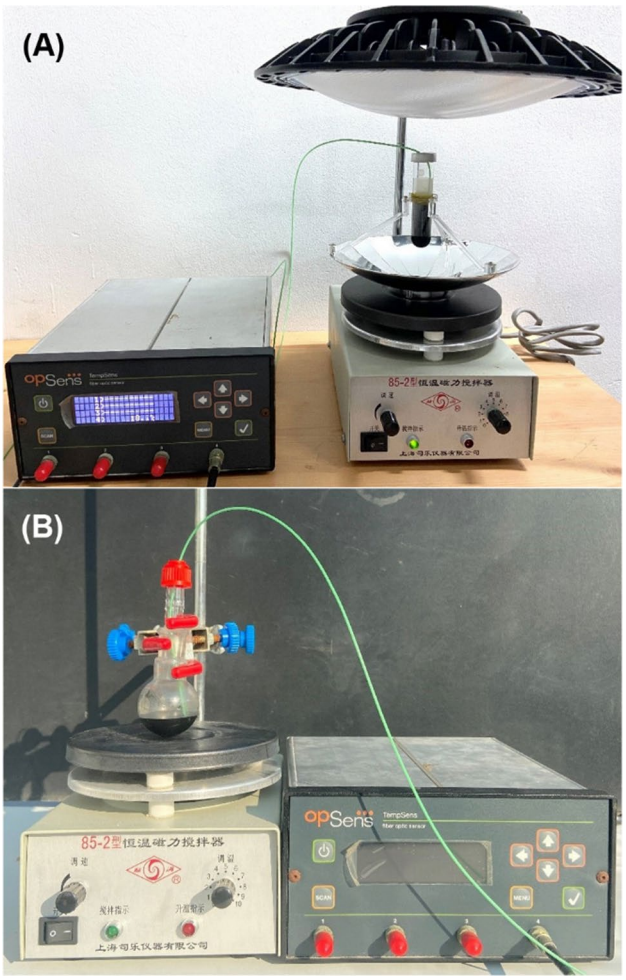


**Fig. 7** Reaction sets for experiments under simulated (**A**) and natural (**B**) sunlight

1,4-dihydropridine scaffold [38, 39]. Therefore, the synthesis of ethyl 5-amino-7-(4-chlorophenyl)-1-[(6-chloropyridin-3-yl)methyl]-8-nitro-1,2,3,7-tetrahydroimidazo[1,2-*a*]-pyridine-6-carboxylate was then chosen as the second model reaction.

The recycling ability is of great importance for the practical application of photothermal catalysts. Under simulated sunlight, the temperature of reaction mixture in first batch and five subsequent runs were kept in a range of 66–68 °C. Some decrease in chemical yield was observed when PEI@GO was reused after several runs; however, when the reaction was carried out for a longer time, a relatively consistent yield could also be achieved (Table 2, entries 1–6). It should be noted that the control experiment without catalyst has been carried out (Table 2, entry 7). No desired product was detected in the absence of PEI@GO.

Due to the continuous variation in weather, the reaction conditions are much intricate under natural sunlight (Fig. 7B). For example, as shown in Fig. 9, the temperature of flask obviously changed in 1 h. However, the model reaction could also be carried out within 18 h in daylight (Table 2, entry 8) [reaction time: 8 h (8:00–16:00) + 8 h (8:00–16:00) + 2 h (8:00–10:00); May 5–7, 2021]. The solar insolation data can be obtained from a professional website established by NASA, USA (https://science.gsfc.nasa.gov/earth/gmao/). These materials are provided in Electronic Supplementary Material (Table S1).

## Adsorption and photothermal desorption of carbon dioxide

After the capacity of polyethylenimine-grafted graphene oxide has been demonstrated in catalysis, we decided to investigate its photothermal regeneration in carbon dioxide capture-and-release processes. It needs to be mentioned that PEI@GO has been reported as an absorbent for $CO_2$ capture

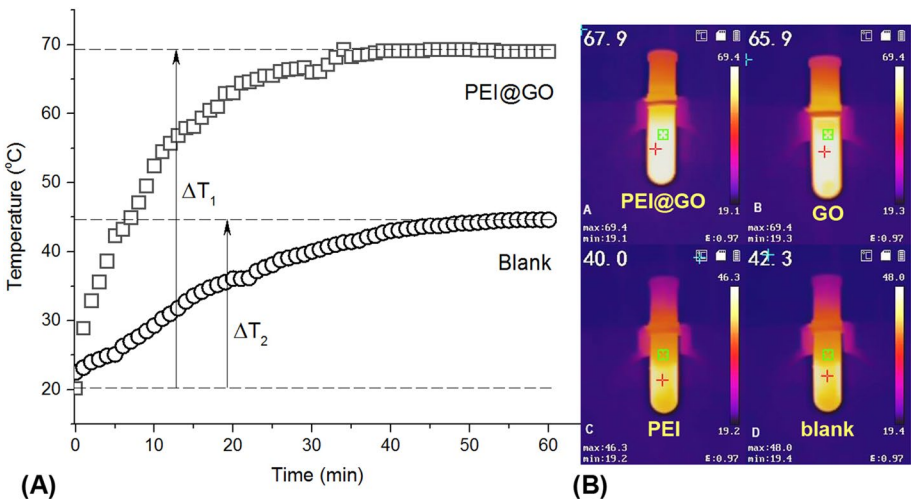


**Fig. 8** **A** Temperature elevation of PEI@GO suspension under simulated sunlight; **B** infrared thermography of reaction vessels

**Table 2** Photothermal synthesis of a neonicotinoid analogue with 1,4-dihydropridine scaffold under simulated and natural sunlight

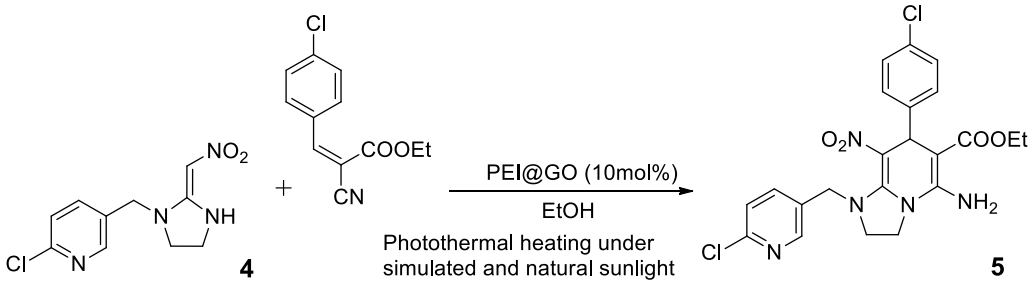


| Entry[a] | Light source | *T*/°C | Time/h | Yield[b]/% |
|---|---|---|---|---|
| 1 | Simulated sunlight | 68 | 7.5 (Run 1) | 70 |
| 2 | Simulated sunlight | 67 | 7.5 (Run 2) | 72 |
| 3 | Simulated sunlight | 67 | 7.5 (Run 3) | 71 |
| 4 | Simulated sunlight | 66 | 8.5 (Run 4) | 70 |
| 5 | Simulated sunlight | 68 | 10.0 (Run 5) | 68 |
| 6 | Simulated sunlight | 67 | 10.0 (Run 6) | 67 |
| 7 | Simulated sunlight | 41 | 7.5 | 0[c] |
| 8 | Natural sunlight | – | 18.0 | 67 |

[a]Reaction conditions: **3** (0.705 g, 3 mmol, 1 eq.), **4** (0.765 g, 3 mmol, 1 eq.), 5 $cm^3$ of EtOH

[b]Isolated yields

[c]In the absence of PEI@GO

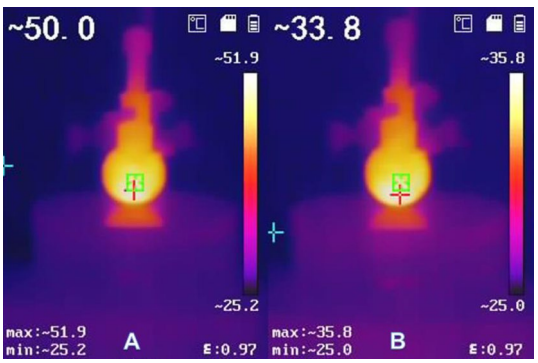


**Fig. 9** Infrared thermography of the flask under natural sunlight

**Table 3** $CO_2$ adsorption capacities of some PEI-based adsorbents under various experimental conditions

| Samples | Conditions | Adsorption capacity/mol/g | References |
|---|---|---|---|
| PEI-GO | 298 K, 1 bar | 1.91 (42.76 $cm^3$/g) | [31] |
| PEI-GO@ZIF-8 | 273 K, 1 bar | 8.08 (181.04 $cm^3$/g) | [40] |
| $SiO_2$/PEI | 298 K, 1 bar | 1.8 | [41] |
| MSiNTs/PEI | 358 K, 1 bar | 2.75 (61.6 $cm^3$/g) | [42] |
| MCM-41/PEI | 348 K, 1 bar | 3.24 | [43] |
| carbon/PEI | 298 K, 1 bar | 1.11 | [44] |
| SWNT/PEI | 348 K, 1 bar | 1.64 | [44] |
| PMMA/PEI | 298 K, 0.02 bar | 0.91 | [44] |
| PEI@GO | 293 K, ~ 1 bar | 1.646 | This work |

[31]. However, the regeneration of PEI@GO has not been investigated based on photothermal desorption.

Selected absorbents based on PEI reported so far in the literature studies are listed in Table 3. In present study, adsorption experiments were carried out at an ambient temperature of 293 K and pressure of 1 bar. A certain amount of PEI@GO was saturated by carbon dioxide in a sealed polypropylene ziplock bag containing dry ice. After 24 h, the static saturated adsorption capacity of $CO_2$ was measured by mass difference method. Five parallel experiments were conducted to ensure the accuracy and stability of the results (1.659 mmol/g, 1.705 mmol/g, 1.614 mmol/g, 1.636 mmol/g, 1.615 mmol/g), while the average value was calculated as 1.646 mmol/g. Hence, the adsorption capacity of PEI@GO prepared in the present study is reasonable in comparison with those data reported in literatures.

The photothermal desorption device based on a small parabolic solar concentrator and open glass bottle charged with $CO_2$-saturated PEI@GO (Fig. 10A). The regeneration experiments were carried out at an ambient pressure of 1 bar under photothermal heating. The temperatures were recorded by infrared thermal imaging camera under full-spectrum LED simulate solar light source (Fig. 10B,

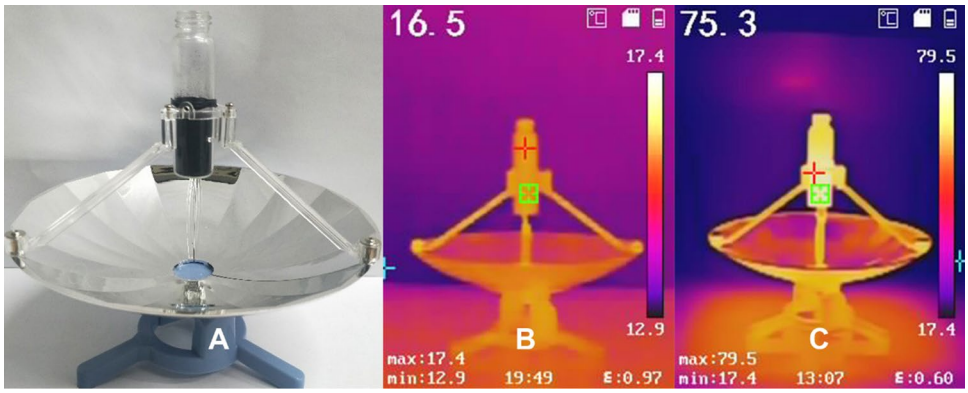


**Fig. 10** Reaction set (**A**) for photothermal desorption of carbon dioxide Infrared thermography of the set in the dark (**B**), or under simulated sunlight (**C**)

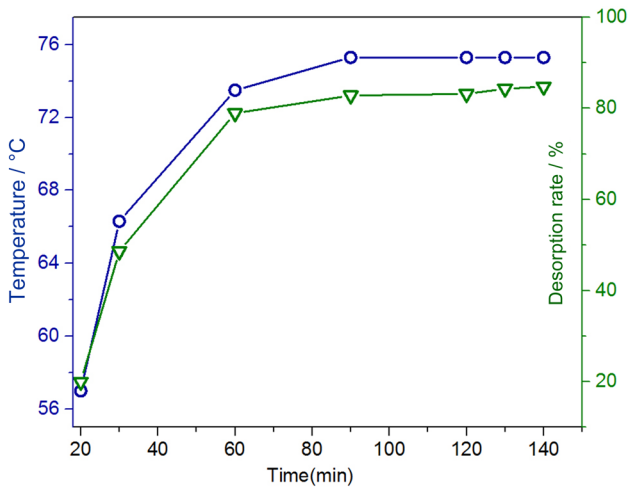


**Fig. 11** Desorption of $CO_2$ under photothermal heating

C). The carbon dioxide desorption rates were calculated by weight loss. The temperature curve under photothermal heating as while as the curve of desorption rate could be shown in Fig. 11. Under simulated sunlight, the temperature of $CO_2$-saturated PEI@GO reach up to 75 °C within 90 min and remain on a plateau. Desorption rate increases rapidly along with increasing temperature. The most of $CO_2$ released from adsorbent in 60 min. Satisfactory result (84%) in regeneration of PEI@GO could be achieved after 2 h.

## Conclusion

The use of solar thermal energy in chemical synthesis is a newly developing area in green chemistry. The present work describes the synthesis, characterization and application of polyethylenimine-grafted graphene oxide as a promising photothermal nanocatalyst in the model reactions. Graphene oxide serves as not only the support of polyethylenimine, but also the absorber of solar energy for photothermal heating. This catalyst is efficient in light-to-heat conversion under visible light and can be easily recycled and reused. Moreover, the use of PEI@GO as an absorbent for carbon dioxide capture-and-release was also investigated based on photothermal regeneration. Further research on the development of new photothermal heterogeneous catalyst based on graphene oxide will be reported in due course.

## Experimental

All chemicals were purchased from commercial suppliers (Shanghai Aladdin Reagent Co. Ltd.) and used without further purification. Graphite was purchased Shanghai Colloid Chemical Plant. The PEI was purchased from Aldrich with an average molecular weight of 600 g/mol. Distilled water was used throughout all the experiments.

FT-IR spectra were taken on a Thermo Nicolet 6700 FT-IR spectrophotometer using KBr pellets. The morphology of PEI@GO was observed by high resolution transmission electron microscopy (HRTEM) using a JEM-2100F apparatus. UV–Vis absorption spectrophotometer (Shimadzu UV-1900) was employed for optical absorbance measurements. XRD patterns were recorded on a Rigaku D/MAX 2550 VB/PC diffractometer with monochromatized Cu $K_\alpha$ radiation at a setting of 40 kV and 100 mA. The thermogravimetric analysis (TGA) of PEI@GO was collected on a Mettler Toledo TGA/SDTA851e thermogravimetric analyzer under $N_2$ atmosphere.

Simulate solar light source (200 W) based on full-spectrum LEDs was purchased from Guangdong Zhongshan CARRY SUN Co.Ltd. The intensity output was measured using a Tenmars (TM-206) Solar Power Meter with a spectral sensitivity range of 400–1100 nm. NIR laser irradiation was performed with a continuous-wave diode NIR laser with a center wavelength of $808 \pm 10$ nm and output power of 8 W (Connect Laser Technology Co., Ltd). The temperature of the solutions was measured by a digital thermometer with thermocouple. Infrared images were recorded by HIK Vision H10 thermal imaging camera. $^1H$ and $^{13}C$ NMR spectra of

organic compounds were measured on a Bruker AC 400 instrument using TMS as an internal standard.

## Preparation of polyethylenimine-grafted graphene oxide

GO was prepared according to the improved Hummer's method [45]. Namely, 69 $cm^3$ of concentrated $H_2SO_4$ in a round bottomed flask was stirred under ice bath for 20 min. $NaNO_3$ (1.5 g) was slowly added into the flask and stir until dissolved completely, followed by 3.0 g of graphite. $KMnO_4$ (9.0 g) was added slowly in portions to keep the reaction temperature below 20 °C. The mixture turned green immediately. On completion, the mixture was warmed to 35 °C and stirred for 7 h, at which time 138 $cm^3$ of water was added slowly, producing a large exotherm above 90 °C. External heating was introduced to maintain the reaction temperature for 20 min, then the heat was removed and the reaction mixture was cooled using a water bath for 10 min. Additional water (420 $cm^3$) and 30% $H_2O_2$ (3 $cm^3$) were added (producing another exotherm). The mixture was cooled to room temperature and centrifuged at 800 rpm. The GO was then washed with 1:10 V/V HCl (10 $cm^3 \times 3$), deionized water (20 $cm^3 \times 3$) and absolute ethanol (20 $cm^3 \times 3$) to remove residual manganese and potassium ions and other impurities by centrifugation. The product was then washed with anhydrous THF, sonicated, and dried under vacuum, yielding graphene oxide.

Vacuum-dried GO (1.5 g) was dispersed in anhydrous THF (15 $cm^3$) and sonicated for 20 min. $SOCl_2$ (25 $cm^3$) was introduced and the mixture refluxed for 24 h. On completion, excess $SOCl_2$ and solvent were removed by rotary evaporation. Functionalized GO reacted with 3 g of PEI in THF (50 $cm^3$) for 24 h under nitrogen atmosphere to obtain PEI@GO.

## Photothermal performance test

PEI@GO was dispersed in ethanol solution with different concentrate (0.1 mg/$cm^3$, 1 mg/$cm^3$, 2 mg/$cm^3$, 5 mg/$cm^3$), stored in quartz cuvettes, then irradiated with NIR laser (wavelength 808 nm, power density 1 W/$cm^2$) for 10 min. The temperature of samples was recorded by a fibre optic thermometer per 2 min (ambient temperature 20 °C).

## Indoor simulations and outdoor tests under natural sunlight

In this experiment, a 200 W full spectrum LED lamp was employed as the light source to simulate the solar light. A small parabolic dish concentrator was placed on the magnetic stirrer, while the LED lamp was suspended vertically. The incident light was concentrated in a relatively small area through the concentrator.

We selected sunny days (May 5–7, 2021) to conduct outdoor experiment on the balcony of the School of Pharmacy, East China University of Science and Technology (Xuhui District, Shanghai, China). The temperature in reaction vessel was monitored by fiber optic thermometers and infrared thermal imaging camera.

## Photothermal catalytic reactions

**Ethyl (*E*)-3-(4-chlorophenyl)-2-cyanoacrylate (3)** PEI@GO (0.14 g, 5%mol) was dispersed in 3 $cm^3$ ethanol by sonication (10 min). 4-Chlorobenzaldehyde (0.28 g, 2 mmol) and ethyl cyanoacetate (0.27 g, 2.4 mmol) were then added. The reaction was first carried out under a solar simulator (428.6 W/$m^2$). The intensity output was measured using an Ambient Weather TM-206 Solar Power Meter with a spectral sensitivity range of 400–1100 nm. During the reaction a foam box was employed for heat preservation. After completion of the reaction, the mixture was cooled to room temperature. The PEI@GO was collected by filtration, and washed with ethanol (5 $cm^3 \times 3$). The crude product was obtained by concentration of filtrate, followed by recrystallization to give 0.441 g (94%) purified white crystals. M.p.: 91–92 °C (Ref. [46] 92–93 °C); $^1$H NMR (400 MHz, DMSO-$d_6$): $\delta = 8.42$ (s, 1H, CH), 8.12–8.03 (m, 2H, Ar–H), 7.73–7.65 (m, 2H, Ar–H), 4.33 (q, $J = 7.1$ Hz, 2H, $CH_2$), 1.32 (t, $J = 7.1$ Hz, 3H, $CH_3$) ppm; $^{13}$C NMR (101 MHz, DMSO-$d_6$): $\delta = 161.58$, 153.64, 137.97, 132.40, 130.20, 129.44, 115.37, 103.21, 62.43, 13.94 ppm.

**Ethyl 5-amino-7-(4-chlorophenyl)-1-[(6-chloropyridin-3-yl)-methyl]-8-nitro-1,2,3,7-tetrahydroimidazo[1,2-*a*]pyridine-6-carboxylate (5)** To a stirred mixture of (*E*)-2-chloro-5-[[2-(nitromethylene)imidazolidin-1-yl]methyl]pyridine (0.77 g, 3 mmol) and (*E*)-3-(4-chlorophenyl)-2-cyanoacrylate (0.71 g, 3 mmol) in EtOH (5 $cm^3$) was add 0.14 g of PEI@GO (5% mol). The reaction was heated for 5 h (monitored by TLC) using a solar simulator (428.6 W/$m^2$). The experiment set was placed in a polystyrene foam box to prevent heat loss. On completion (monitored by TLC), the solvent was removed under reduced pressured to afford the crude product. Purification by recrystallization from ethanol gave 1.031 g (70% yield) of light yellow solid was obtained. M.p.: 207–208 °C; $^1$H NMR (400 MHz, DMSO-$d_6$): $\delta = 8.22$ (d, $J = 2.4$ Hz, 1H, Ar–H), 7.73–7.48 (m, 3H, Ar–H), 7.28–7.11 (m, 3H, Ar–H), 7.02–6.92 (m, 2H, Ar–H), 5.15 (s, 1H, Ar–H), 4.73 (q, $J = 15.7$ Hz, 2H, $CH_2$), 4.19–3.99 (m, 4H, $NCH_2CH_2N$), 3.96 (q, $J = 7.1$ Hz, 2H, $CH_2$), 1.07 (t, $J = 7.0$ Hz, 3H, $CH_3$) ppm; $^{13}$C NMR (151 MHz, DMSO-$d_6$): $\delta = 168.04$, 153.09, 150.63, 149.98, 149.53, 144.97, 139.34,

131.37, 130.86, 128.85, 128.19, 124.27, 107.82, 79.80, 59.06, 51.45, 51.01, 43.36, 38.83, 14.84 ppm; HRMS (EI): *m/z* calc. for $C_{22}H_{21}Cl_2N_5O_4$ 489.0971, found 489.0969.

## Adsorption and photothermal desorption of carbon dioxide

The $CO_2$ adsorption/desorption property of PEI@GO was characterized through the difference method. Experiments were carried out at an ambient temperature of 293 K and pressure of 1 bar. 1.000 g of PEI@GO was spread in a culture dish which was sealed in polypropylene ziplock bag containing dry ice (24 h). The static saturated adsorption capacity of $CO_2$ was measured by mass difference method. Five parallel experiments were conducted to ensure the accuracy and stability of the results. The desorption device based on a small parabolic solar concentrator and transparent glass bottle charged with $CO_2$-saturated PEI@GO. The temperatures were recorded by infrared thermal imaging camera under full-spectrum LED simulate solar light source. The amount of carbon dioxide desorption was measured by weight loss.

**Supplementary Information** The online version contains supplementary material available at https://doi.org/10.1007/s00706-023-03055-6.

**Acknowledgements** Financial support from the National Key Research and Development Plan (SQ2017ZY060054) is gratefully acknowledged.

**Data availability** The spectroscopic data of the products are available in the Supplementary Information.

## References

1. Lewis NS, Nocera DG (2006) Proc Natl Acad Sci USA 103:15729
2. Jung HS, Verwilst P, Sharma A, Shin J, Sessler JL, Kim JS (2018) Chem Soc Rev 47:2280
3. Lal S, Clare SE, Halas NJ (2008) Acc Chem Res 41:1842
4. Zhu L, Gao M, Peh CKN, Ho GW (2018) Mater Horiz 5:323
5. Sun X, Jiang S, Huang H, Li H, Jia B, Ma T (2022) Angew Chem Int Ed 61:e202204880
6. Du S, Bian X, Zhao Y, Shi R, Zhang T (2022) Chem Res Chin Univ 38:723
7. Cheng P, Wang D, Schaaf P (2022) Adv Sustain Syst 6:2200115
8. Mulvaney P (1996) Langmuir 12:788
9. Baffou G, Quidant R (2014) Chem Soc Rev 43:3898
10. Mehta P, Barboun P, Go DB, Hicks JC, Schneider WF (2019) ACS Energy Lett 4:1115
11. Wang F, Li C, Chen H, Jiang R, Sun L, Li Q, Wang J, Yu JC, Yan C (2013) J Am Chem Soc 135:5588
12. Long R, Rao Z, Mao K, Li Y, Zhang C, Liu Q, Wang C, Li Z, Wu X, Xiong Y (2015) Angew Chem Int Ed 54:2425
13. Jia J, O'Brien PG, He L, Qiao Q, Fei T, Reyes LM, Burrow TE, Dong Y, Liao K, Varela M, Pennycook SJ, Hmadeh M, Helmy AS, Kherani NP, Perovic DD, Ozin GA (2016) Adv Sci 3:1600189
14. Robinson JT, Tabakman SM, Liang Y, Wang H, Casalongue HS, Vinh D, Dai H (2011) J Am Chem Soc 133:6823
15. Li Z, Lei H, Kan A, Xie H, Yu W (2021) Energy 216:119262
16. Yeh C, Wu P, Chen D (2014) Mater Lett 136:274
17. Dai Y, Zhu M, Wang X, Wu Y, Huang C, Fu W, Meng X, Sun Y (2018) Nanotechnology 29:245703
18. Zhang Y, Guo H, Weng W, Fu M (2017) Phys Chem Chem Phys 19:31389
19. Shin HH, Yang W, Lim D (2019) Carbon 143:362
20. Xiao Y, Liu J, Wang H, Yang C, Cheng H, Deng Y, Cheng L, Fang Y (2020) Mol Catal 493:111103
21. Wang J, Zhang G, Zhang P (2018) Appl Catal B Environ 239:77
22. Nguyen DT, Truong R, Lee R, Goetz SA, Esser-Kahn AP (2014) Energy Environ Sci 7:2603
23. Wang Q, Luo J, Zhong Z, Borgna A (2011) Energy Environ Sci 4:42
24. Gunathilake C, Jaroniec M (2015) J Mater Chem A 3:2707
25. Gunathilake C, Manchanda AS, Ghimire P, Kruk M, Jaroniec M (2016) Environ Sci Nano 3:806
26. Gunathilake C, Dassanayake RS, Kalpage CS, Jaroniec M (2018) Materials 11:2301
27. Gunathilake C, Dassanayake RS, Fernando CAN, Jaroniec M (2022) J Compos Sci 6:168
28. Hummers WS, Offeman RE (1958) J Am Chem Soc 80:1339
29. Chen W, Yan L, Bangal PR (2010) J Phys Chem C 114:19885
30. Paredes JI, Villar-Rodil S, Martinez-Alonso A, Tascon JMD (2008) Langmuir 24:10560
31. Shin G, Rhee K, Park S (2016) Int J Hydrogen Energy 41:14351
32. Blanton TN, Majumdar D (2013) Powder Diffr 28:68
33. Aboutalebi SH, Chidembo AT, Salari M, Konstantinov K, Wexler D, Liu HK, Dou SX (2011) Energy Environ Sci 4:1855
34. Xu Q, Shen Y, Zhang Y, Shao X (2019) Bioorg Med Chem Lett 29:2398
35. Yuan C, Chen W, Yan L (2012) J Mater Chem 22:7456
36. Wang F, Cheng Z, Tan J, Yuan Y, Yong S, Liu L (2017) Renew Sustain Energy Rev 79:1314
37. Matsuda K, Buckingham SD, Kleier D, Sattelle DB (2001) Trends Pharmacol Sci 22:573
38. Zhang W, Yang X, Chen W, Xu X, Li L, Zhai H, Li Z (2010) J Agric Food Chem 58:2741
39. Li Z, Qian X, Yang X, Xu X, Tao L, Song G (2010) Heterocyclic nitrogenous compounds with insecticidal activity and their preparation, agrochemical compositions and use in the protection of crops and animals. Patent WO 2010075760A1, Jul 8, 2010; (2010) Chem Abstr 153:116215
40. Huang A, Feng B (2018) Int J Hydrogen Energy 43:2224
41. Fang Q, Wang H (2020) Mater Res Express 7:035026
42. Niu M, Yang H, Zhang X, Wang Y, Tang A (2016) ACS Appl Mater Interfaces 8:17312
43. Xu X, Song C, Miller BG, Scaroni AW (2017) Ind Eng Chem Res 44:8113
44. Shoi SC, Drese JH, Jones CW (2010) Chemsuschem 2:796
45. Marcano DC, Kosynkin DV, Berlin JM (2010) ACS Nano 4:4806
46. Bakhtiari K, Haghighi M, Derikvand F (2006) Lett Org Chem 3:297